THE JOURNAL OF PHYSICAL CHEMISTRY A

Article

Imaging the State-Specific Vibrational Predissociation of the CH–NH Hydrogen-Bonded Dimer

Jessica A. Parr, Guosheng Li, Igor Fedorov, Anthony J. McCaffery, and Hanna Reisler

J. Phys. Chem. A, **2007**, 111 (31), 7589-7598• DOI: 10.1021/jp070838+ • Publication Date (Web): 02 June 2007

Imaging the State-Specific Vibrational Predissociation of the $C_2H_2-NH_3$ Hydrogen-Bonded Dimer

Jessica A. Parr,[†] Guosheng Li,[†] Igor Fedorov,[†] Anthony J. McCaffery,[‡] and Hanna Reisler*,[†]

Department of Chemistry, University of Southern California, Los Angeles, California 90089-0482, Department of Chemistry, University of Sussex, Brighton BN19QJ, United Kingdom

Received: January 31, 2007; In Final Form: April 3, 2007

The state-to-state vibrational predissociation (VP) dynamics of the hydrogen-bonded ammonia−acetylene dimer were studied following excitation in the asymmetric CH stretch. Velocity map imaging (VMI) and resonance-enhanced multiphoton ionization (REMPI) were used to determine pair-correlated product energy distributions. Following vibrational excitation of the asymmetric CH stretch fundamental, ammonia fragments were detected by 2 + 1 REMPI via the $\tilde{B}^1E'' \leftarrow \tilde{X}^1A_1'$ and $\tilde{C}'^1A_1' \leftarrow \tilde{X}^1A_1'$ transitions. The fragments' center-of-mass (c.m.) translational energy distributions were determined from images of selected rotational levels of ammonia with one or two quanta in the symmetric bend (ν_2 umbrella mode) and were converted to rotational-state distributions of the acetylene co-fragment. The latter is always generated with one or two quanta of bending excitation. All the distributions could be fit well when using a dimer dissociation energy of $D_0 = 900 \pm 10$ cm^{-1}. Only channels with maximum translational energy <150 cm^{-1} are observed. The rotational excitation in the ammonia fragments is modest and can be fit by temperatures of 150 ± 50 and 50 ± 20 K for $1\nu_2$ and $2\nu_2$, respectively. The rotational distributions in the acetylene co-fragment pair-correlated with specific rovibrational states of ammonia appear statistical as well. The vibrational-state distributions, however, show distinct state specificity among channels with low translational energy release. The predominant channel is $NH_3(1\nu_2) + C_2H_2(2\nu_4$ or $1\nu_4 + 1\nu_5)$, where ν_4 and ν_5 are the trans- and cis-bend vibrations of acetylene, respectively. A second observed channel, with much lower population, is $NH_3(2\nu_2) + C_2H_2(1\nu_4)$. No products are generated in which the ammonia is in the vibrational ground state or the asymmetric bend ($1\nu_4$) state, nor is acetylene ever generated in the ground vibrational state or with CC stretch excitation. The angular momentum (AM) model of McCaffery and Marsh is used to estimate impact parameters in the internal collisions that give rise to the observed rotational distributions. These calculations show that dissociation takes place from bent geometries, which can also explain the propensity to excite fragment bending levels. The low recoil velocities associated with the observed channels facilitate energy exchange in the exit channel, which results in statistical-like fragment rotational distributions.

1. Introduction

Since the first definitive description of the hydrogen bond by Pauling in the 1930s,[1] there has been much interest in understanding the nature, role, and dynamics of the hydrogen bond in diverse environments. Many theoretical studies have been carried out on hydrogen-bonded systems with interest in both strong and weak hydrogen bonds.[2a,b] In the gas phase, emphasis has been placed on studying hydrogen-bonded dimers in the cold environment of supersonic expansions. Spectroscopic work, especially at high resolution, has naturally focused on line widths and frequency shifts, correlating them with predissociation rates. Roger Miller was one of the first to extend the spectroscopic work to state-to-state dynamics of the predissociation of hydrogen-bonded dimers between two molecules, using the HF dimer and dimers of acetylene with hydrogen halides as benchmark cases.[3−7] It has been recognized early on that the disparity between the frequencies of the intermolecular and intramolecular vibrational modes causes energy transfer in the complex to be inefficient, thereby leading to nonstatistical predissociation.

Most of the available data on state-specific effects in energy flow in predissociation of dimers have been obtained with molecule−atom or diatom−diatom dimers. For two polyatomic molecules, state-specific information on energy disposal is scarce, and in the few cases that have been studied, acetylene has often served as one of the monomers.[8−11] Acetylene can engage in hydrogen bonds with acids via its π-bond, and with strong bases via its weakly acidic hydrogen. Previous work in which acetylene served as the Lewis base in T-shaped dimers with HF, HCl, and OH demonstrated a strong preference for populating the CC stretch of the acetylene fragment following excitation of the asymmetric CH stretch.[8−11] This energy flow pattern is apparently encouraged by a near resonance in the acetylene monomer between one quantum of the asymmetric CH stretch and the CC stretch plus two quanta of bend.

In this paper, we report the first vibrational predissociation (VP) study of a complex of acetylene with the polyatomic base ammonia. In this dimer, acetylene acts as a Lewis acid whose hydrogen is bonded to the nitrogen of ammonia, a strong Lewis base. From previous experimental[12−14] and theoretical[15,16] work, it was deduced that the acetylene−ammonia dimer has a linear geometry typical of a traditional hydrogen bond. The intermolecular bond, however, is expected to be fairly weak due to the

* Corresponding author. E-mail: reisler@usc.edu.
[†] Department of Chemistry, University of Southern California.
[‡] Department of Chemistry, University of Sussex.

10.1021/jp070838+ CCC: $37.00
Published on Web 06/02/2007

low acidity of acetylene, and theory predicts a binding energy between 778 and 920 cm^{-1}.[15,16]

Following asymmetric CH stretch excitation, we used velocity map imaging (VMI) to obtain energy distributions of the acetylene fragment correlated with specific rovibrational states of ammonia. We also determined mode-specific vibrational excitation in the fragments and the hydrogen bond dissociation energy, D_0. The most intriguing finding of this study is that both dissociation fragments are produced with vibrational excitation distributed in a very specific way. Ammonia fragments are always generated vibrationally excited with one or two quanta of the umbrella (symmetric bending) mode, ν_2, while the bending levels $1\nu_4$ or $1\nu_4 + 1\nu_5$ are excited in C_2H_2. This leaves very little energy to be distributed between rotation and translation. Other combinations of fragment states that provide pathways with low translational energy release are not populated. These are: (i) ground-state ammonia and acetylene with one quantum of the CC stretch ν_2, (ii) ground-state ammonia and acetylene with three quanta of bend, ν_4 and ν_5, in various combinations, and (iii) ground-state acetylene and ammonia with one quantum of the asymmetric bend ν_4.

Information on the geometry, spectroscopy, and intermolecular modes of the dimer is essential for explaining energy flow pathways in VP. The origin band of the asymmetric CH stretch fundamental of the acetylene−ammonia dimer is at 3213.6 cm^{-1}, red-shifted by ~75 cm^{-1} from the origin of the asymmetric CH stretch in free acetylene.[13] The spectrum has a well-resolved rotational structure, indicating that the lifetime of the vibrationally excited complex is longer than a rotational period (>0.1 ns).[13] The same absorption feature was seen in the FTIR study of the acetylene−ammonia dimer reported by Lin et al.[14] In neither study was the NH stretch of ammonia in the dimer observed, although the ammonia umbrella mode was isolated by Lin et al.[14] A microwave study determined that the dimer has a small rotational constant, 0.091 cm^{-1}, and a hydrogen bond length of 2.33 Å between the nitrogen on ammonia and the hydrogen on acetylene.[12] No work has been reported on the VP dynamics of this dimer.

Spoliti et al. carried out electronic structure calculations and obtained a hydrogen bond length of 2.340 Å, intermolecular stretching frequency of 124 cm^{-1}, and a binding energy of 11 kJ/mol (919.6 cm^{-1}).[15] Hartmann and Radom, who carried out more recent electronic structure calculations, assigned a linear structure to the dimer and determined a binding energy of 9.3 kJ/mol (777.5 cm^{-1}). The bond lengths calculated for atoms not directly involved in hydrogen bonding were r(C−H) = 1.063 Å, r(C≡C) = 1.209 Å, r(N−H) = 1.013 Å, and the ammonia bond angles are 106.7°. For the atoms directly involved in the hydrogen bond, the bond lengths predicted were r(C−H) = 1.072 Å, with a hydrogen bond length of 2.280 Å.[16] Lin et al. also used ab initio methods to determine the intermolecular vibrational modes and geometric parameters of the dimers. They obtained a hydrogen bond length of 2.2852 Å, an H−N−H angle of 112.32°, and intermolecular vibrational modes of 125 cm^{-1} for the stretching frequency, and 208 and 74 cm^{-1} for the bending frequencies.[14] The dimer geometry is shown in Figure 1.

In interpreting the experimental findings, we are hindered by the absence of a potential energy surface (PES) for the acetylene−ammonia dimer. We can, however, rationalize the results by an analysis based on two approximate models whose value has been established by successful application to dimers ranging from atom−diatom to two polyatomic molecules. One model has been presented by Ewing,[17,18] who combined the momentum (or energy) gap law with the requirement that the number of quanta transferred in the dissociation be minimized. This model predicts correctly the predissociation rate of a large variety of complexes and explains why the preferred predissociation pathway involves small translational energy release. A complementary angular momentum (AM) model, proposed by McCaffery and co-workers and based on momentum interconversion, has been used extensively to describe inelastic collisions[19] and, more recently, predissociation of weakly bound dimers.[19,20] By determining the principal geometries from which dissociation occurs, it can also help in understanding the observed modes of vibrational excitation.

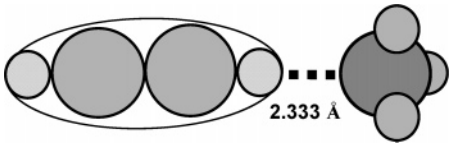

Figure 1. Space-filling model of the ammonia acetylene dimer. Hydrogen bond length: 2.333 Å;[12] N−H bond length: 1.013 Å;[16] C−H (non-hydrogen-bonding) bond length: 1.063 Å;[16] C≡C bond length: 1.209 Å;[16] C−H (hydrogen-bonding) bond length: 1.072 Å.

The method of analysis employed here to describe the rotational distributions is that introduced by McCaffery and Marsh[20] and is based on the AM model of inelastic and dissociative processes.[19] In this approach, the motive force originates in momentum change (dp/dt) and for many events at the molecular level consists of conversion of linear momentum into orbital angular momentum and molecular rotation. This critical process takes place about a lever arm or effective impact parameter (b_n) shown from experiment to be of the order of molecular dimension,[21] being half bond length in a homonuclear diatomic and an equivalent distance from the molecule's center-of-mass (c.m.) in a heteronuclear species.[19] Molecules may be represented by hard shapes having size and mass distribution that reflect their physical shape. Input data for quantitative calculations consist of bond lengths, mass, and spectroscopic constants, and thus a PES is not required for momentum exchange calculations. However, in calculating probability distributions, it is important that the chosen hard shape should give an accurate representation of the key probability distribution $P(b_n)$ for a large number of random trajectories.[19] The three-dimensional ellipsoid has been found to be very useful in this respect.[19,20,22]

A limitation of the AM model in describing VP of weakly bound complexes is that often the amount of energy available for disposal in rotation and translation is quite small, as most of the energy is deposited in fragment vibrations. As a consequence, the fragments have low recoil velocities, facilitating further energy exchange in the exit channel. In such a case, calculations using hard-shape potentials may not provide quantitative descriptions of the rotational/translational energy distributions but rather give insight as to preferred dissociation geometries and average amounts of energy in rotation vs translation. Nevertheless, when combined with structural and spectroscopic information, the AM model has successfully described rotational/translational energy disposal in many inelastic, reactive, and VP processes.[19] It is in this spirit that it is used in the present work.

The paper is organized as follows. In Section 2, we describe the experimental methods and procedures, and in Section 3, we present the experimental results and the analyses used to obtain the pair-correlated rovibrational fragment distributions. In Section 4, the results of the AM model calculations of the correlated rotational distributions of acetylene are described, and

in Section 5, the VP mechanism is discussed with special emphasis on state-specific effects. A summary is provided in Section 6.

2. Experimental Details

In this experiment, VMI was used in conjunction with 2 + 1 resonance-enhanced multiphoton ionization (REMPI) to detect fragments from the vibrational predissociation of the ammonia−acetylene dimer. The state-selected translational energy distributions were analyzed to determine the dynamics and energy transfer in the VP of the dimer.

The dimers were formed in a pulsed supersonic molecular beam by expanding a mixture of 20% acetylene (Airgas, dissolved in acetone) and 1% ammonia (Matheson, anhydrous 99.99%) in He (Gilmore, 99.9999%) at a stagnation pressure of ~2 atm through a 0.5 mm orifice of a pulsed valve. The acetylene was separated from the acetone that is added to prevent polymerization by trap-to-trap distillation at the temperature of a CO_2/ethanol slush bath (195 K). The concentrations of acetylene and ammonia were carefully optimized to minimize contamination from larger clusters, especially $(NH_3)_n$. The molecular beam was collimated by a skimmer (1.0 mm orifice, Beam Dynamics) before intersecting at right angles two counter-propagating laser beams in the interaction region.

Unfocused infrared (IR) laser radiation (5 mJ) was used to excite the asymmetric CH stretch of the dimer (~3213 cm^{-1}), and focused (40 cm) frequency-doubled ultraviolet (UV) radiation (0.8 mJ) was used to detect state-selected ammonia fragments from the vibrational predissociation of the dimer. The IR radiation was generated by an OPO/OPA system (Laser Vision, 18−22 mJ at 2700−3400 cm^{-1}; 0.4 cm^{-1} bandwidth). The UV radiation was generated by a dye laser (Continuum ND 6000, DCM) pumped by a Nd:YAG laser (Spectra Physics, GCR 230). The timing of the lasers was fixed by a delay generator (Stanford, DG535), which was controlled through a GPIB interface (National Instruments). Spectra were collected by alternating "IR on" and "IR off" conditions. In "IR on", the IR laser fires 20 ns before the UV laser, whereas in "IR off", the IR laser is fired 1 μs after the UV laser.

The lasers were timed to monitor the leading part of the molecular beam pulse where the population of dimers was the largest. The rotational temperature of the clusters was estimated at 5 K by monitoring the origin band of the $\tilde{B}\ ^1E'' \leftarrow \tilde{X}\ ^1A^{1\prime}$ system of monomer ammonia by 2 + 1 REMPI.[23] The UV spectra were modeled using the program PGOPHER developed by Western.[24] Vibrationally excited ammonia fragments were detected through the same $\tilde{B}$ state in the range 342.1−347.8 nm and through the $\tilde{C}'$ ($^1A_1'$) state in the range 313−321.5 nm. A mixture of 20% C_2H_2 and 1% NH_3 in Ne at 2 atm stagnation pressure was also used in an attempt to better cool the ammonia monomer background.

The VMI arrangement has been described in detail previously.[25,26] In brief, it consists of a four-lens ion acceleration assembly, a 60 cm field free drift tube, and a CCD camera (LaVision, Imager) that monitors a phosphor screen, coupled to an MCP detector (BURLE Electro-Optics Co.). In this experiment, two modes were used to collect data: (i) time-of-flight (TOF) mass spectrometry for spectroscopic investigations and (ii) VMI mode for determining center of mass (c.m.) translational energy distributions. The two-dimensional projections were collected using an event counting method and reconstructed to three-dimensional images by using the BASEX method,[27] which also provided the translational energy distributions. The energy distributions were converted to c.m. translational energy distributions by using momentum conservation and analyzed to determine the internal energy of the acetylene co-fragments as well as the dissociation threshold of the acetylene−ammonia dimer.

3. Results and Analysis

Two Rydberg states were exploited in investigating the REMPI spectra of the ammonia fragments, the $\tilde{B}^1E''$ and $\tilde{C}'^1A_1'$ states. Three types of data were collected: (i) REMPI spectra of ammonia fragments resulting from VP of the dimer, (ii) IR action spectra of the excited dimer, and (iii) photofragment ion images of state-selected ammonia fragments. First, the results obtained via the $\tilde{B}$ state are presented, followed by the $\tilde{C}'$ state studies.

1. Detection via the $\tilde{B}\ ^1E''$ State of NH_3. *A. REMPI Spectroscopy of Ammonia Fragments.* In this experiment, the asymmetric CH stretch of the dimer, whose band origin is at 3213.6 cm^{-1}, is excited while monitoring selected rovibrationally excited ammonia fragments through the $\tilde{B}\ ^1E''$ state. The IR laser is set at 3214.3 cm^{-1}, the frequency giving the highest intensity in the R-branch of the acetylene asymmetric CH stretch. Figure 2 shows 2 + 1 REMPI spectra of ammonia obtained via the $\tilde{B}$ state in the region of excitation of the symmetric bending (umbrella) mode, ν_2, with the IR laser on and off. The only NH_3 fragments detected are vibrationally excited in one or two quanta of ν_2. No other vibrational levels are observed even though $1\nu_4$, the asymmetric bend, is energetically accessible. No ammonia fragments are observed in the vibrational ground state even upon further cooling with Ne to ~2 K to decrease the contribution from background rotationally excited ammonia.

Figure 2 also shows spectral simulations from which the rotational temperature (T_{rot}) of the vibrationally excited ammonia fragments is estimated from best fits.[24] The $2^0_{1^+}$ band is best fit with $T_{rot} = 150 \pm 50$ K, with a maximum at $J'' = 3$, whereas the $2^0_{2^+}$ band is fit well with $T_{rot} = 50 \pm 20$ K with a maximum at $J'' = 1$. The average rotational energy of NH_3 in $1\nu_2^+$ and $2\nu_2^+$ at temperatures of 150 and 50 K, respectively, is 103 and 35 cm^{-1}, and the available energy allows rotational states in $1\nu_2^+$ and $2\nu_2^+$ states of ammonia of up to $J'' = 11$ and 6, respectively (see below). Simulations intended to examine selectivity in K-state populations (e.g., by assuming only $K'' = 0$ or $K'' = J''$) show that the best fits are obtained when both J and K are assumed to have Boltzmann distributions. Note that the integrated intensity of the $2^0_{1^+}$ band is much higher than that of the $2^0_{2^+}$ band with a ratio of $2^0_{1^+}:2^0_{2^+} = 25:1$.

Ammonia has a low barrier to inversion in the ground state (~2020 cm^{-1}),[28] and the vibrational wavefunctions are split into ν_2^+ and ν_2^- components. The only component that could be observed via the $\tilde{B}$ state was ν_2^+. This is most likely a result of spectroscopic selection rules and band overlap, but dynamical considerations cannot be ruled out a priori. The missing ν_2^- vibrational state can also be accessed via the $\tilde{C}'$ state, as described below.

B. Infrared Action Spectra. Figure 3 shows a typical IR action spectrum obtained by monitoring the $2^0_{1^+}$ [$^rS_0(1)$] transition and scanning the IR frequency. The Q branch of the IR transition is not observed because of the C_{3v} symmetry of the dimer. The unresolved rotational structure in the spectrum is a result of the large bandwidth of the IR laser (0.4 cm^{-1}), and the spectrum is consistent with spectra obtained previously.[13,14]

The spectrum was fit as a b-type transition using the molecular constants derived by Hilpert et al.[13] The shoulders labeled $(NH_3)_x$ and $(NH_3)_y$ are from ammonia clusters. Similar

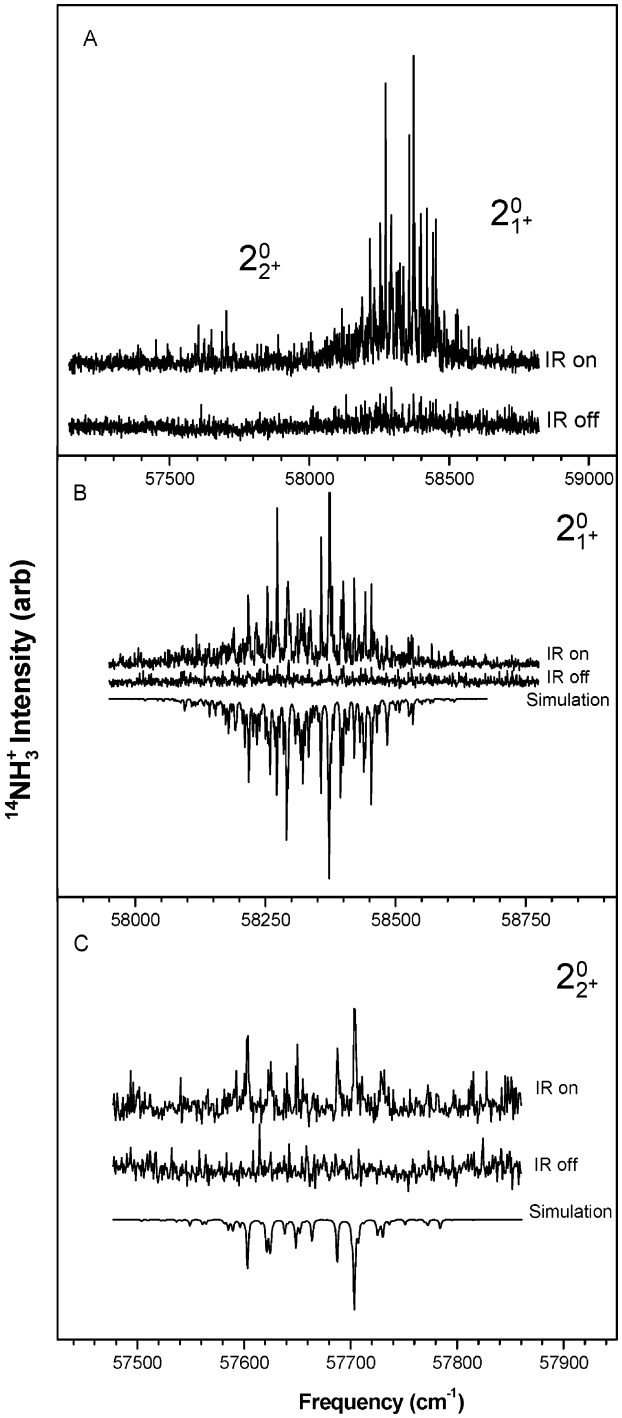

Figure 2. (A) NH_3 photofragment 2 + 1 REMPI spectrum obtained by pumping the R branch of the asymmetric CH stretch of the dimer at 3214.3 cm^{-1} and scanning the REMPI laser to excite the $\tilde{B}^1E''(0) \leftarrow \tilde{X}^1A_1'(1\nu_2^+, 2\nu_2^+)$ transition with IR on and IR off. (B) A simulation of the $2^0_{1^+}$ band of the spectrum in A using the PGOPHER program (ref 24) with $T_{rot} = 150$ K. (C) A simulation of the $2^0_{2^+}$ band with $T_{rot} = 50$ K.

IR absorptions of ammonia clusters were observed by Slipchenko et al.[29] in He droplet studies and Lin et al.[14] in gas-phase studies in the same frequency range. In the current study, IR excitation at 3214.3 cm^{-1} was chosen for photofragment studies of NH_3 because there is less contamination from larger ammonia clusters at this energy and therefore the majority of the ammonia fragments result from the acetylene−NH_3 dimer. Similar action spectra were observed when monitoring other (J'', K'') states of ammonia.

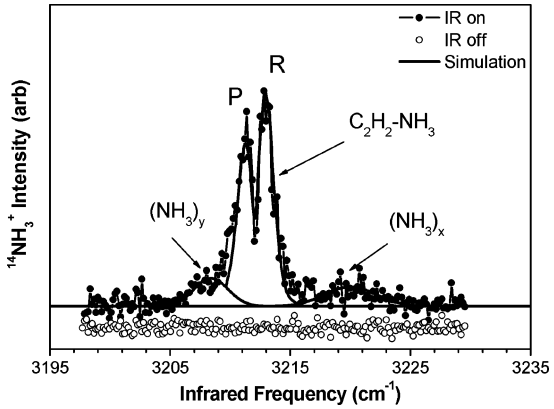

Figure 3. Photofragment yield spectrum of NH_3 obtained by monitoring the $2^0_{1^+}$ [$^rS_0(3)$] transition while scanning the IR frequency. The simulation shown as the solid line is a fit obtained with molecular parameters of ref 5. The labels $(NH_3)_y$ and $(NH_3)_x$ indicate absorption of ammonia clusters of unknown sizes.

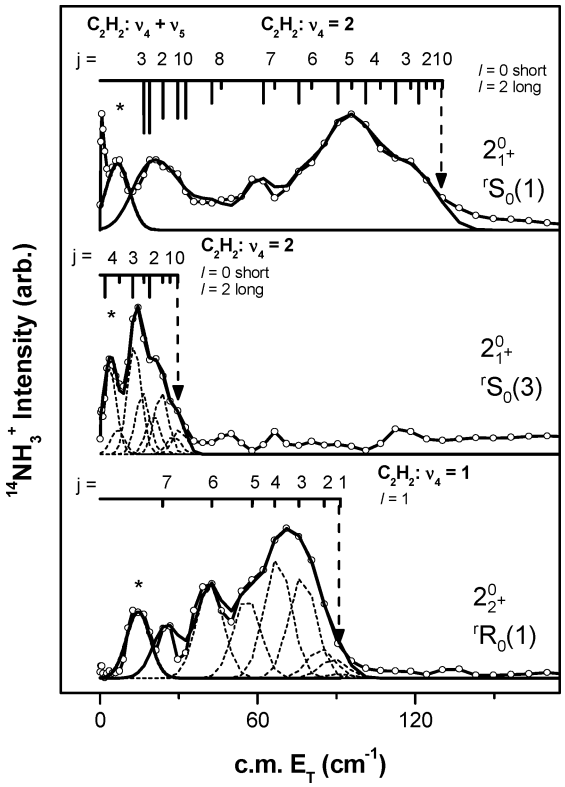

Figure 4. Translational energy distributions (c.m.) of the fragments obtained by monitoring the $2^0_{2^+}$ [$^rR_0(1)$], $2^0_{1^+}$ [$^rS_0(3)$], and $2^0_{1^+}$ [$^rS_0(1)$] transitions of NH_3 via the $\tilde{B}$ state following excitation of the R branch of the asymmetric CH asymmetric stretch of the dimer at 3214.3 cm^{-1} are shown as open circles. The distributions were obtained from reconstructions of the 2D NH_3 images. The acetylene co-fragment vibrational and rotational states are labeled above the sticks indicating the center positions of the Gaussians used in the fits (shown in dotted lines). The best fits are shown as solid lines (see the text for details). The low-energy peaks labeled by (∗) are artifacts and are not considered in the fitting process. The arrows indicate the maximum available translational energy assuming a bond dissociation energy $D_0 = 900 \pm 10$ cm^{-1}.

C. Ion Imaging Results. The c.m. translational energy distributions shown in Figure 4 were obtained from ion images collected with the IR frequency fixed at 3214.3 cm^{-1} and the UV frequency fixed on a specific rovibrational state of the ammonia fragment. To determine the correlated internal state

distributions of the acetylene fragment, conservation of energy was used:

$$h\nu = D_0 + E_T + E_{vib}(NH_3) + E_{vib}(C_2H_2) + E_{rot}(NH_3) + E_{rot}(C_2H_2)$$

where hν is the photon energy used for vibrational excitation of the dimer, D_0 is the dissociation energy of the dimer, E_T is the c.m. translational energy, $E_{vib}(NH_3)$ and $E_{vib}(C_2H_2)$ are the vibrational energies of ammonia and acetylene, respectively, and $E_{rot}(NH_3)$ and $E_{rot}(C_2H_2)$ are the corresponding rotational energies. D_0, $E_{vib}(C_2H_2)$, and $E_{rot}(C_2H_2)$ are unknown, whereas state-selective REMPI designates the state of the ammonia fragment, $E_{rot}(NH_3) + E_{vib}(NH_3)$, and E_T is determined from the images. To obtain images, we selected J'', K'' levels of NH_3 that are least overlapped by other transitions. D_0 was determined by fitting all the measured translational energy distributions with a single dissociation energy. The fit was accomplished by using a sum of Gaussian functions whose positions were determined by the rovibrational state of the acetylene co-fragment, and their width was 8 cm^{-1}, held constant throughout the fitting process.

The lowest trace in Figure 4 depicts the c.m. translational energy distribution obtained by monitoring ammonia with two quanta of ν_2^+ via the $^rR_0(1)$ line. Assuming that the acetylene co-fragment has one quantum of vibrational energy in ν_4 (trans-bend) and $D_0 = 900 \pm 10$ cm^{-1}, we obtain rotational excitation up to $j'' = 7$ in acetylene. The middle trace corresponds to ammonia fragments with one quantum of excitation in ν_2^+ monitored via the $^rS_0(3)$ line. Using the same D_0 as before, the acetylene co-fragments are now found to have two quanta of vibrational excitation in ν_4 and rotational excitation up to $j'' = 4$. Because acetylene is a linear molecule and the trans-bend mode is degenerate, *l*-type doubling must be included,[30] as manifested here as well as in the top trace, which depicts the corresponding c.m. translational distribution obtained by monitoring $1\nu_2^+$ via the $^rS_0(1)$ line. The top trace exhibits a bimodal distribution that is best fit by two different bending vibrations of acetylene. Two quanta of ν_4 fits the higher translational energy part, whereas $1\nu_4 + 1\nu_5$ fits the part with lower translational energy. *l*-type doubling is included in fitting both $2\nu_4$ and $1\nu_4 + 1\nu_5$, and rotational excitation up to $j'' = 8$ is observed in the acetylene fragment.

Note that the c.m. translational energy in the three traces does not exceed 140 cm^{-1}, demonstrating the well-known propensity in complexes for producing fragments with vibrational excitation that minimizes translational energy release (see below).[17] The best fits for the middle and bottom traces are obtained with $D_0 = 900 \pm 10$ cm^{-1} and are unique. The fit for the top trace may not be unique because of the large number of acetylene rovibrational states accessed, but $D_0 = 900 \pm 10$ cm^{-1} is consistent with the fit shown.

The lowest energy peaks labeled * are artifacts of the experimental method. This is confirmed by recording an image of NH_3 in a molecular beam with no acetylene present and no vibrational excitation. When the image is reconstructed, the peak at ~10 cm^{-1} still appears, as well as a large peak at 0 cm^{-1}, which is expected for NH_3 with no recoil energy. Thus, the artifact may be due either to the analysis method or to a contamination in NH_3. The signal intensities in these experiments are very low (especially in cases when the product population is spread over many quantum states) because low monomer concentrations are required to suppress formation of large clusters. Nevertheless, only in the middle trace is there a direct overlap between the artifact peak and a rotational state of acetylene. In this fit, the contribution from the fragments could not be distinguished from the contribution of the artifact, leading to greater uncertainty in the relative population of that state.

TABLE 1: Relative Populations of Acetylene Rovibrational States upon VP Following Excitation of the CH Asymmetric Stretch. The Populations are Normalized to a Sum of 1.

NH_3 (vib state)	C_2H_2 (vib state)	E_T (cm^{-1})	C_2H_2 (j)	C_2H_2 (l)	relative populations[a]
$1\nu_2^+$ $^rS_0(3)$	$2\nu_4$	29.5	0	0	0.07 (0.03)
		27.1	1	0	0.04 (0.03)
		22.4	2	0	0.15 (0.03)
		19.4	2	2	0.10 (0.02)
		15.3	3	0	0.15 (0.03)
		12.2	3	2	0.26 (0.05)
		5.9	4	0	0.06 (0.01)
		2.7	4	2	0.19 (0.19)
$2\nu_2^+$ $^rR_0(1)$	$1\nu_4$	86.9	1	1	0.04 (0.008)
		82.2	2	1	0.06 (0.01)
		75.2	3	1	0.20 (0.04)
		65.8	4	1	0.24 (0.05)
		54.0	5	1	0.16 (0.03)
		39.9	6	1	0.18 (0.04)
		23.5	7	1	0.11 (0.02)

[a] The numbers in parentheses are error estimates. The relative populations could be changed by ~20% without significantly changing the fit.

Table 1 lists the vibrational and rotational states populated in the acetylene co-fragments derived from the translational energy distributions obtained by imaging ammonia fragments via the 2^0_{1+} [$^rS_0(3)$] and 2^0_{2+} [$^rR_0(1)$] transitions. Images obtained by monitoring the ammonia 2^0_{1+} [$^rS_0(1)$], 2^0_{1+} [$^qS_0(0)$], 2^0_{2+} [$^qS_0(0)$], and 2^0_{1-} [$^qS_0(0)$] transitions were also obtained. They show a behavior consistent with that displayed in Figure 4, but the correlated acetylene rotational distributions are not listed because the fits are less accurate, especially for those levels showing bimodal distributions. The accuracy and reproducibility of the data are sufficient, though, to identify the vibrational levels of the acetylene co-fragment.

The best fits for the bimodal distributions always show that the peak with higher translational energy corresponds to two quanta of ν_4 excitation in the acetylene co-fragment, and the peak with lower translational energy corresponds to a combination of one quantum of ν_4 and one quantum of the cis-bend, ν_5. In all cases, the data are fit well with $D_0 = 900 \pm 10$ cm^{-1}, and the available energy is partitioned into vibrational states that minimize c.m. translational energy with a relatively small number of rotational levels excited in the ammonia and acetylene fragments.

2. Excitation of NH_3 Fragments via the $\tilde{C}'^1A_1'$ State. REMPI photofragment spectra of NH_3 via the $\tilde{C}'(^1A_1')$ state were exploited to further probe the dynamics and, in particular, look for the missing vibrational component, ν_2^-.[23] To confirm that the ammonia signal observed via the $\tilde{C}'$ $1\nu_2 \leftarrow \tilde{X}$ $1\nu_2^-$ transition results from excitation of the acetylene−ammonia dimer, an IR action spectrum was taken by monitoring specific rovibronic transitions in NH_3. A typical spectrum is shown in Figure 5; its shape is similar to the one shown in Figure 3.

A. REMPI Spectroscopy. Figure 6 shows REMPI spectra of ammonia fragments resulting from VP of dimers excited at 3214.3 cm^{-1}. The $1\nu_2^+$, $2\nu_2^+$, and $1\nu_2^-$ vibrational states are all observed. The 2^1_{1-} transition is the only one involving $1\nu_2^-$ that can be observed because the 2^0_{1-} transition is forbidden. We conclude that both the $1\nu_2^+$ and $1\nu_2^-$ components of ν_2 are generated in the photolysis, and $2\nu_2^-$ cannot be excited because of insufficient energy.

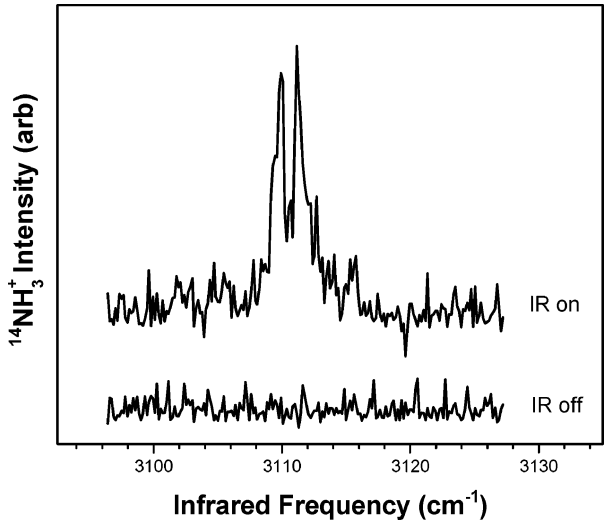

Figure 5. Photofragment yield spectrum of NH_3 obtained by monitoring the $^qS_0(0)$ rotational line of the $\tilde{C}'^1A_1'(1\nu_2) \leftarrow \tilde{X}^1A_1'(1\nu_2^-)$ transition while scanning the IR frequency.

In fitting the rotational transitions, we find that, as a result of the selection rule $\Delta J = \pm 2$ and the low rotational excitation, only the $^qS_0(0)$ rotational line is significantly populated for all three vibrational states. This makes it impossible to determine the rotational temperature except to say that it is probably less than 100 K because states with $J'' \geq 2$ have too low an intensity to be identified clearly above the background. This is consistent with the results obtained by monitoring ammonia fragments via the $\tilde{B}$ state. We note that when probing the $\tilde{C}'$ state, only $\Delta J = \pm 2$ transitions are allowed, whereas in probing the $\tilde{B}$ state $\Delta J = 0, \pm 1$ and ± 2 are allowed.

B. Ion Imaging Results. The c.m. translational energy distributions correlated with ammonia fragments that have one quanta of ν_2^+ or ν_2^- are shown in Figure 7. Both the shapes and the maximum translational energies are similar to those obtained via the $\tilde{B}$ state (Figure 4), supporting the vibrational assignments in the acetylene and ammonia fragments. The small differences in maximum available energies between the results shown in Figures 3 and 6 are due to differences in the rotational and vibrational energies of the monitored ammonia fragments. The $\tilde{B}$ state $^qS_0(0)$ line could not be spectroscopically isolated, and the fragment monitored through the $^qS_0(1)$ line (Figure 4) has $\sim$10 cm^{-1} less energy available than in the corresponding trace shown in Figure 7. The $1\nu_2^-$ state lies $\sim$35 cm^{-1} higher in energy than the $1\nu_2^+$ state, leaving less energy for translation and decreasing the maximum available energy. The bimodal structure suggests similar assignments for the acetylene co-fragments correlated with the 2^0_{1+} and 2^1_{1-} transitions. The peak at $\sim$10 cm^{-1}, labeled by *, is again an artifact of the experimental method as described above.

4. Calculations of Rotational Distributions

Models based on classical scattering from hard shape potentials have been quite successful in describing many processes involving energy transfer. In particular, a classical model that takes into account kinematic considerations can pinpoint angular momentum constraints that may limit the extent of linear to angular momentum conversion. In the inelastic collision, only the normal component $\mathbf{p}_n$ of the linear momentum $\mathbf{p}$ can be converted to angular momentum, and in the case of a homonuclear diatomic, the associated impact parameter b_n is given by the perpendicular line that connects $\mathbf{p}_n$ with the c.m.

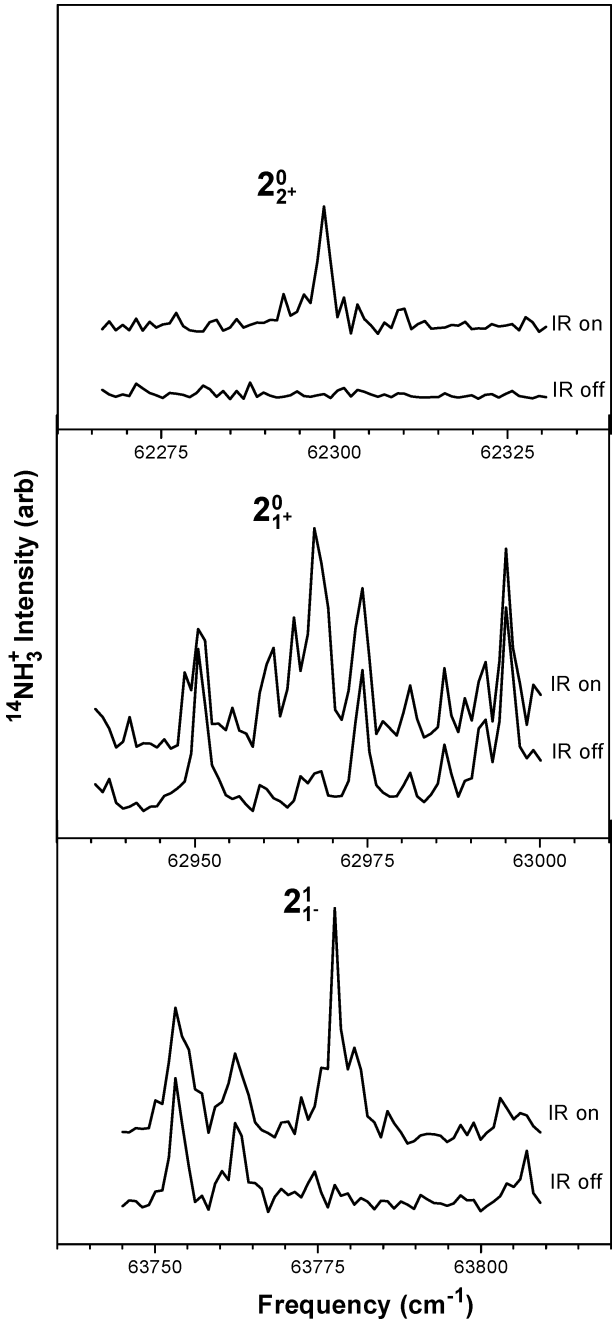

Figure 6. NH_3 photofragment 2 + 1 REMPI spectra obtained by pumping the R branch of the asymmetric CH stretch of the dimer at 3214.3 cm^{-1} and scanning in the region of the $\tilde{C}'^1A_1'(0) \leftarrow \tilde{X}^1A_1'$-$(1\nu_2^+, 1\nu_2^-, 2\nu_2^+)$ transitions with IR on and IR off. The upper, middle, and lower panels show the 2^0_{2+}, 2^0_{1+}, and 2^1_{1-} transitions, respectively. The other peaks belong to the $\tilde{B} \leftarrow \tilde{X}$ transition.

of the ellipsoid.[22] This method is extended to dimers of polyatomic molecules by introducing the concept of the equivalent rotor, a rigid ellipsoid having the moment of inertia and major axis length of the molecule it represents along the inertial axis, giving rise to a particular *J*- or *K*-changing transition.[31,32] A more detailed description is given in a forthcoming publication.[33] In this model, *J*- and *K*- changing transitions in NH_3 are treated separately, while in the case of acetylene, a single hard ellipsoid based on molecular dimensions is appropriate for calculating its pair-correlated rotational distributions. Information on the relative orientations of the fragment molecules at the moment of dissociation is contained in the maximum allowed value of the effective impact parameter

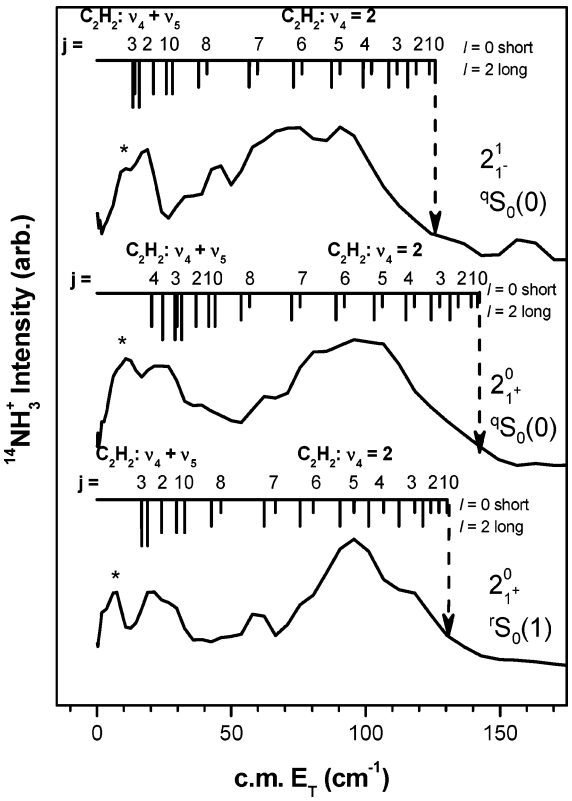

Figure 7. Translational energy distributions (c.m.) of the fragments obtained by monitoring the 2^0_{1+} [$^rS_0(1)$] transition of NH_3 via the $\tilde{B}$ state and the 2^0_{1+} [$^qS_0(0)$] and 2^1_{1-} [$^qS_0(0)$] transitions of NH_3 via the $\tilde{C}'$ state following excitation of the R branch of the asymmetric CH stretch of the dimer at 3214.3 cm^{-1}. The distributions were obtained from reconstructions of the 2D NH_3 images. The acetylene co-fragment vibrational and rotational states are labeled above the sticks indicating the center positions of the Gaussians used in the fits (not shown). The low-energy peaks labeled by (∗) are artifacts and are not considered in the fitting process. The arrows indicate the maximum available translational energy assuming a bond dissociation energy $D_0 = 900 \pm 10$ cm^{-1}.

(b_n^{max}) required to fit the experimental data. Studies that examine such collisions show that the dimensions of the hard shape potentials are similar to those of the colliding molecules and that b_n is close to half bond length in a diatomic molecule.

In the AM model of VP, dissociation is assumed to result from an "internal collision" between the weakly bound fragments.[20,31] Thus, the range of "collision" geometries is limited compared to an inelastic collision. This effectively restricts b_n^{max} in the conversion of linear momentum into orbital and rotational AM of the fragments. In reality, a fairly wide range of b_n values is usually accessed, resulting from stretching and bending motions of the weak intermolecular bond.[20,31] The conversion of these large amplitude motions, in particular bending vibrations, into rotational excitation, can explain the appearance of rotational excitation in both acetylene and ammonia fragments.

Once the equivalent rotor has been specified, calculation of rotational distributions in the fragment species requires only the energy available to distribute between rotation and translation (E_{RT}) within the specified fragment vibrational manifold together with standard spectroscopic data. In the AM model, information on the relative orientations of the fragment molecules at the moment of dissociation (the point of contact on the ellipsoid surfaces) is contained in the values of b_n^{max} required to fit the experimental data. The maximum available value is set by the parameters of the equivalent rotor, being for example 1.51 Å for C_2H_2, and this provides an upper limit for calculations in which b_n^{max} is varied. Note that this quantity determines the peak and width of the rotational distribution. In VP, its value is dependent on stereochemical factors, particularly the point of contact on the ellipsoid surfaces, and it yields information on the orientation of each species at the moment of dissociation. The characteristic rotational distribution for a given b_n^{max} resembles a Boltzmann distribution that is truncated sharply beyond the maximum *j*-value allowed by available energy.[20] In attempting to reproduce the data, in each case, the minimum number of discrete values of b_n^{max} was chosen (≤ 2) that gives a reasonable fit to the data. This procedure therefore identifies the *principal* VP sites in the complex at the moment of dissociation.

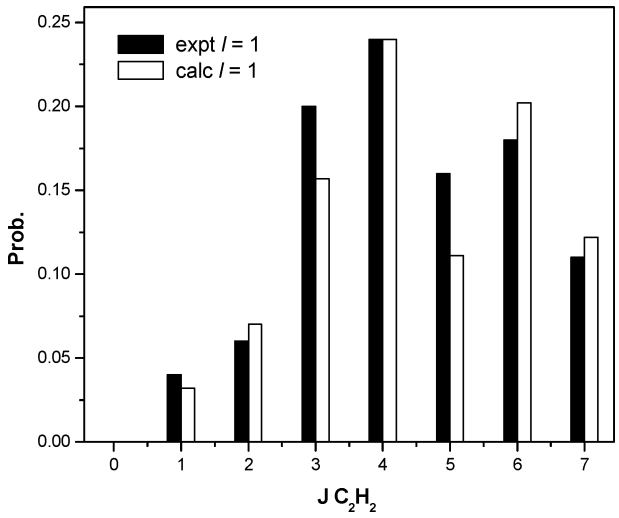

Figure 8. Calculated and experimental rotational distributions in the ν_4 mode of C_2H_2 coincident with $2\nu_2^+$; $^rR_0(1)$ of NH_3. Two values of b_n^{max} were used to fit the data, namely 0.64 and 1.2 Å.

1. NH_3 Rotational Distributions. NH_3 is excited with one or two quanta of ν_2^+, the umbrella mode. For the observed correlated acetylene bending states, energy conservation dictates that the maximum *J* state in ammonia is 11 for $1\nu_2^+$ and 6 for $2\nu_2^+$. The experimental distributions peak at much lower *J*'s, i.e., 3 and 1 for $1\nu_2^+$ and $2\nu_2^+$, respectively. Calculations on the ammonia fragment indicate that these *J* levels result from an impact on NH_3 at a point 0.08 ± 0.02 Å along the NH bond (measured from the center of the N atom) when $1\nu_2^+$ is excited and 0.05 ± 0.02 Å in the case of 2 ν_2^+. Thus, the collision can be envisaged as hitting the N atom of NH_3 slightly off-center, simultaneously exciting the umbrella mode in ammonia and bending levels in acetylene, as well as some rotation. The hit is a little closer to the center of the N atom when 2 quanta of the vibrational mode are excited compared to when $1\nu_2^+$ is populated with consequent effects on the maximum *J* states.

2. Correlated C_2H_2 Rotational Distributions. The rotational distributions of Figure 4 indicate that VP to the bend modes of acetylene, $2\nu_4$ and $1\nu_4 + 1\nu_5$, is facile with dissociation occurring from more than one geometry. Calculated and experimental rotational distributions in the C_2H_2 fragments correlated with specific NH_3 rovibrational states are displayed in Figures 8−10. Agreement is generally good, although in each case, it is evident that by including a greater number of dissociation geometries, a better fit could be obtained. However, as exit-channel interactions between the two fragments may alter the nascent rotational distributions, our objective is to obtain a reasonable fit with the minimum number of dissociation sites in order to glean insight into the principal mechanisms of

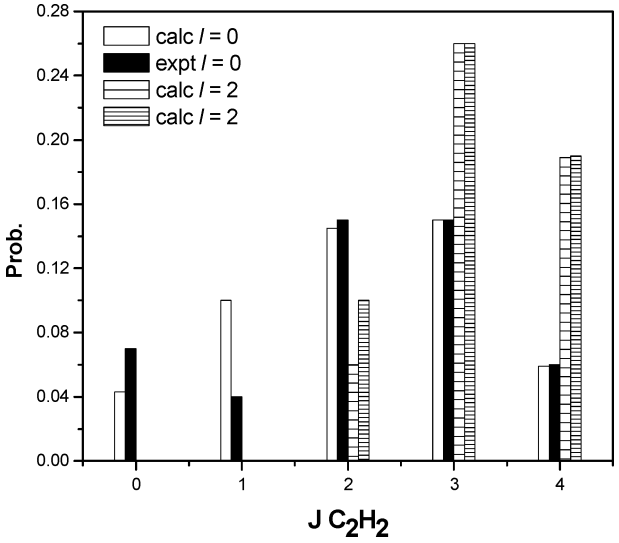

Figure 9. Calculated and experimental rotational distributions in the $2\nu_4$ mode of C_2H_2 $l = 0$ and $l = 2$ coincident with $1\nu_2^+$; $^rS_0(3)$ of NH_3. For the $l = 2$ calculations $b_n^{max} = 1.1$ Å, while for $l = 0$, two values 0.5 and 0.94 Å were needed.

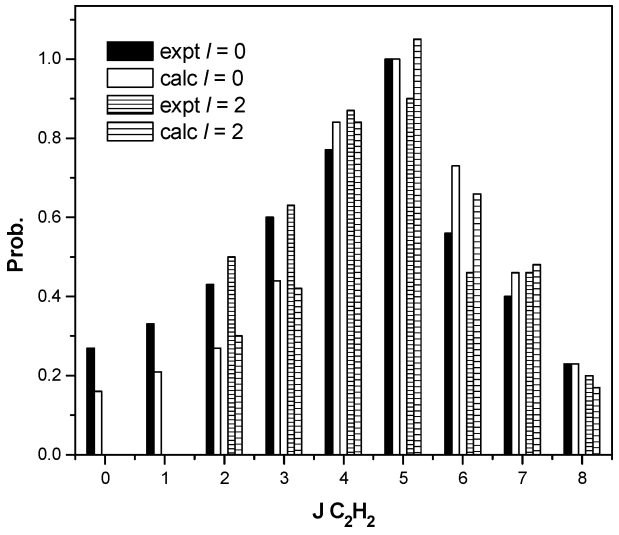

Figure 10. Calculated and experimental rotational distributions in the $2\nu_4$ mode of C_2H_2, $l = 0$ and $l = 2$, coincident with $1\nu_2^+$; $^rS_0(1)$ of NH_3. For $l = 0$ calculations, $b_n^{max} = 0.6$ Å, while for $l = 2$, two values 0.6 and 0.8 Å were needed.

TABLE 2: Values of b_n^{max} Used to Fit Rotational Distributions in NH_3 and C_2H_2

NH_3		C_2H_2		
vib level	b_n^{max} (Å)	vib level	l	b_n^{max} (Å)
$2\nu_2^+$ $^rR_0(1)$	0.05	$1\nu_4$	1	0.64; 1.2
$1\nu_2^+$ $^rS_0(3)$	0.08	$2\nu_4$	0	0.5; 0.94
			2	1.1
$1\nu_2^+$ $^rS_0(1)$	0.08	$2\nu_4$	0	0.58
			2	0.58, 0.8

dissociation. In the plots shown, no more than two values on b_n^{max} were used for each data set, and in some instances, just one sufficed. Three sets of data are displayed corresponding to the correlated distributions (i) Figure 8, $NH_3(2\nu_2^+; {}^rR_0(1))$; C_2H_2-$(1\nu_4)$; (ii) Figure 9, $NH_3(1\nu_2^+; {}^rS_0(3))$; $C_2H_2(2\nu_4; l = 0,2)$; (iii) Figure 10, $NH_3(1\nu_2^+; {}^rS_0(1))$; $C_2H_2(2\nu_4; l = 0,2)$. Table 2 lists the b_n^{max} values used to obtain the data shown in each of these experimental cases. Note that when two vibrational quanta of C_2H_2 are acceptor modes, data in states with vibrational angular momentum $l = 2$ and $l = 0$ were treated separately.

Case (i). $NH_3(2\nu_2^+; {}^rR_0(1))$; $C_2H_2(1\nu_4; l = 0, j)$. The disposal of energy into the $2\nu_2^+$; $^rR_0(1)$ state of the NH_3 fragment leaves around 700 cm^{-1} to be partitioned between internal states of C_2H_2 and recoil, but as can be seen from Figure 4, the majority of the available energy is disposed as vibrational motion. The acceptor vibration in VP must be excited simultaneously with rotation, and in acetylene, the ν_4 trans-bend mode clearly meets this requirement. Similar criteria are found to influence the vibrational relaxation of the 6^1 S_1 level of benzene.[32]

The calculations provide a good fit to the experiment, as shown in Figure 8. Values of $b_n^{max} = 1.2$ and 0.64 Å are responsible for the dominant peaks at $j'' = 6$ and 4, respectively. These b_n^{max} correspond to dissociation geometries involving a bent hydrogen bond. Two intermolecular bend modes are predicted for this complex,[14] having frequencies 208 and 74 cm^{-1}, as well as a hydrogen-bond stretch of 125 cm^{-1}. The higher value of b_n^{max} corresponds to a greater degree of bend than the lower, and this may reflect the fact that the motion of the two bend modes gives rise to impact at two different sites. Impact is at the same point on the NH_3 fragment in both instances.

Case (ii). $NH_3[1\nu_2^+; {}^rS_0(3)]$; $C_2H_2(2\nu_4; l = 0, 2, j)$. In this instance, a greater amount of energy is deposited in NH_3 rotation than in the previous case, and furthermore, two quanta of ν_4 are excited in the correlated C_2H_2 fragment. This leaves very little remaining energy to be disposed into C_2H_2 rotation and recoil. The pattern of disposal in this case is quite complex, with $l = 2$, 0 levels accessible in $2\nu_4$. Figure 9 shows calculated and experimental rotational intensities separately for $l = 0$ and for $l = 2$. The fit is good, and for $l = 2$, only a single b_n^{max} value was required of length 1.1 Å, indicating dissociation from a point away from the end of the C_2H_2 ellipsoid. The $l = 0$ data are spread over the full range of accessible energy. Two b_n^{max} values, 0.5 and 0.94 Å, were required to obtain a fit that is satisfactory at high j values but less good at low j. The very small translational energy released in this case, however, should facilitate energy transfer in the exit channel, resulting in a broader (statistical-like) distribution than would have been generated by an impulsive collision.

Case (iii). $NH_3[1\nu_2^+; {}^rS_0(1)]$; $C_2H_2(2\nu_4; l = 0, 2, j)$. This set of data differs from case (ii) above only in the rotational level of the monitored NH_3 state and, consequently, there is a larger amount of energy and momentum to be disposed as C_2H_2 rotation and recoil. The distribution shown in Figure 4 is quite complex, and a unique fit of the experimental data using Gaussians was not possible. Here a more qualitative approach is taken than in the previous two cases in that the experimental and calculated data refer to peak values in the distribution rather than the magnitudes of the Gaussians as in cases (i) and (ii). Calculated fits do not provide as good a match to experiment in this instance as in those cases considered earlier, especially for low j values (see Figure 10). The fit parameters obtained in this case are $b_n^{max} = 0.6$ Å for the $l = 0$ data and $b_n^{max} = 0.6$ and 0.8 Å for $l = 2$.

5. Discussion

The ammonia−acetylene dimer exhibits many properties characteristic of vdW clusters, but at the same time its VP shows distinct fingerprints of state-specific behavior in vibrational energy disposal. As is common in vdW clusters, the VP rate is slow, and the preferred pathways are those that minimize translational energy release. On the other hand, the predisso-

TABLE 3: Energy Available to Rotation and Translation upon Vibrational Predissociation of the Dimer Following Excitation of the CH Asymmetric Stretch[a]

E_v (cm^{-1})	NH_3 vibration	HCCH vibration	$E_{RT} = E_{avail} - E_v$ (cm^{-1})
1974.3	0000	01000	339.1
1855.7	0000	$0003^1 0$	457.7
1861.9	0000	$0003^3 0$	451.5
1941.2	0000	$000(21)^1$ II	372.2
1960.9	0000	$000(21)^1$ I	352.5
2049.1	0000	$000(12)^1$ II	264.3
2067.0	0000	$000(12)^1$ I	246.4
2170.3	0000	00003^1	143.1
2198.0	0000	00003^3	115.4
2239.9	0001	$0001^1 0^0$	73.5
2162.8	01^+00	$0002^0 0^0$	150.6*
2166.0	01^+00	$0002^2 0^0$	147.5*
2260.5	01^+00	$000(11)^{+0}$	52.9*
2273.0	01^+00	$000(11)^{-0}$	40.4*
2280.0	01^+00	$000(11)^2$	33.5*
2198.5	01^-00	$0002^0 0^0$	114.9*
2201.6	01^-00	$0002^2 0^0$	111.8*
2296.2	01^-00	$000(11)^{+0}$	17.2*
2308.7	01^-00	$000(11)^{-0}$	4.7*
2210.6	02^+00	$0001^1 0^0$	102.8*

[a] $E_{avail} = E_{CHstretch} - D_0 = 2313.4$ cm^{-1}. Observed Channels are denoted by *. The vibrational frequencies for the trans- and cis- bends of acetylene are $\nu_4 = 612.9$ cm^{-1} and $\nu_5 = 730.3$ cm^{-1}, respectively,[30] and the symmetric stretch of acetylene is $\nu_2 = 1974.3$ cm^{-1}.[34] The vibrational frequencies for ammonia symmetric bend are $1\nu_2^+ = 932.5$ cm^{-1}, $1\nu_2^- = 968.3$ cm^{-1}, and $2\nu_2^+ = 1597.6$ cm^{-1}.[28]

ciation is state specific when it comes to vibrational modes, with several channels with fairly low translational energy release clearly disfavored. The predominant vibrational channels are $NH_3(1\nu_2^+, 1\nu_2^-) + C_2H_2(2\nu_4$ and $1\nu_4 + 1\nu_5)$, and their population is much larger than the other observed channel, $NH_3(2\nu_2^+) + C_2H_2(1\nu_4)$ (ratio greater than 25:1). All channels with $NH_3(v = 0)$, including the $NH_3(v = 0) + C_2H_2(1\nu_2)$ (which dominates the VP of T-shaped acetylene dimers),[8-11] the $NH_3(v = 0) + C_2H_2$ with a total of three quanta in bending motions in various combinations, as well as $NH_3(1\nu_4) + C_2H_2(v = 0)$ are not observed although they fulfill the criteria proposed by Ewing.[17,18] Table 3 lists the possible combinations of acetylene and ammonia vibrational excitations that are accessible for $E_{vib} + E_{rot} + E_T = h\nu - D_0 = 2314$ cm^{-1} and would result in low (<500 cm^{-1}) translational energy release.

The vibrational state-specificity may be related to the low probability of predissociation. With a dissociation lifetime >0.1 ns, the CH asymmetric stretch lives for many periods of oscillation before coupling (directly or indirectly) to the C−H−N intermolecular coordinate. In other words, the coupling matrix elements are all small and must be strongly dependent on internal collision geometry and impact parameter.

The rationale given for the momentum gap law in VP is that minimizing the momentum gap maximizes the overlap between the intermolecular stretch wave function and the fast oscillating translational wavefunction of the departing fragments. However, this description does not take into account angular momentum conservation, which demands that the sum of the orbital angular momentum generated by the dissociating impulse emanating from CH vibration plus parent angular momentum must equal $\mathbf{J_{NH3}} + \mathbf{j_{C2H2}} + \boldsymbol{l}$. This conversion is often constrained by the kinematics of the collision and is best computed by using the AM model described above.

To minimize momentum gap in VP, vibrational excitation of the fragments is favored because it can dispose of most of the available energy as internal energy. The total requirements on the dissociating system are therefore quite severe: it has to simultaneously minimize momentum gap and satisfy angular momentum conservation, while at the same time the excited CH vibration must couple to other vibrational levels of the monomers. This required confluence may explain why dissociation is so slow and why it is hard to treat theoretically: an accurate PES that can pinpoint favored dissociation geometries is unavailable, the matrix elements are all small, and the intermolecular motions have large amplitudes.

The results obtained in the present study show that the dimers find only limited ways to dispose of the rather large amount of energy released by relaxation of the CH stretch vibration. The fraction of the available energy deposited in rotation and translation is modest, and thus the requirements on momentum and energy conservation are easily satisfied. Fits of the rotational distributions by the AM model with a hard ellipsoid potential indicate that the impact leading to dissociation occurs mostly from bent geometries, explaining the appearance of some rotational excitation in the products. As orbital and rotational angular momenta are generated simultaneously with vibrational excitation in *both* ammonia and acetylene, the internal collision must excite specific vibrations, while at the same time imparting torque to the departing fragments. This limits the favored impact geometries, as seen in the calculations. The maximum translational energy release, however, is quite small, ranging from 70 to 150 cm^{-1} for the different channels, and thus the associated maximum relative velocities are only 2−5 Å per ps. These long separation times allow for energy exchange in the exit channel, explaining the statistical-like rotational distributions in the acetylene co-fragment. This, and the floppy nature of the complex, also explain why there is no preferred axis of rotation, as demonstrated by the Boltzmann distribution of both J and K states of ammonia.

The most striking result of the present study is the strong state-specificity in vibrational energy disposal. The predominant VP pathways have *both* NH_3 and C_2H_2 carrying vibrational excitation. However, three channels, one involving NH_3 in the asymmetric bend ν_4, another involving three quanta of the bends in acetylene, and the third having C_2H_2 with one quantum of ν_2 (CC stretch), are absent even though they involve modest translational energy release and a small number of transferred quanta. The ammonia ν_4 mode is probably discriminated against because of geometrical constraints in the dimer's VP. It is hard to imagine a feasible geometry and impact parameter of the dimer that would lead to excitation of the asymmetric bend. Likewise, it is difficult to imagine a geometry that would lead preferentially to a transfer of three quanta of bending to the acetylene fragment.

The CC stretch is the mode predominantly excited in the VP of dimers of acetylene with HX (X = F, Cl, O) following CH stretch excitation. These complexes, however, are all T-shaped with a hydrogen bond between the H of HX and the π bond of acetylene. To break this hydrogen bond requires energy flow from the excited CH stretch of acetylene through the CC stretch and bend modes to the intermolecular bond that involves the π system of acetylene. The near-resonance between the CH stretch and two quanta of acetylene bend plus one quantum of CC stretch facilitates such energy flow toward the VP reaction coordinate. In contrast, in the linear CH−N hydrogen bond of the ammonia−acetylene dimer, exciting the CC bond takes energy in a direction away from the reaction coordinate and may hinder rather than facilitate VP. Apparently, energy transfer across the intermolecular bond, which involves simultaneous excitation of bend modes in both the NH_3 and C_2H_2 moieties, is the preferred route from the bent geometries of the dimer

that lead to most of the VP. CC stretch excitation may also be disfavored because the energy available to rotation and translation would be $\sim$340 cm^{-1}, significantly larger than in the observed pathways.

6. Summary

The predissociation dynamics of the ammonia−acetylene dimer following excitation of the CH stretch fundamental vibration were studied using VMI at the pair correlation level. The dissociation energy of the hydrogen-bonded dimer is $D_0 = 900 \pm 10$ cm^{-1}, and the dissociation rate is slow. Although energy disposal follows the general guidelines proposed by Ewing in which translational energy release is small and the number of transferred quanta is minimized, the predissociation is state specific with regard to vibrational energy disposal. The main predissociation channel is $NH_3(1\nu_2) + C_2H_2(2\nu_4$ or $1\nu_4 + 1\nu_5)$, and a minor channel, $NH_3(2\nu_2) + C_2H_2(1\nu_4)$, is also observed, i.e., only channels with energy transfer across the hydrogen bond. No other channels are observed, although more channels with low translational energy release are open (Table 3). No ammonia or acetylene fragments are formed in the ground vibrational state, and dissociation of the hydrogen bond always gives rise to vibrational excitation in *both* fragments. Rotational excitation is low: the ammonia fragments have rotational temperatures of 150 and 50 K for $1\nu_2$ and $2\nu_2$ vibrational levels, respectively. Estimates of impact parameters obtained with the AM model by using hard shape potentials show that dissociation takes place predominantly from bent geometries of the complex, which may explain the propensity for bending excitations in the products. The low c.m. recoil velocity facilitates energy exchange in the exit channel, giving rise to Boltzmann-like rotational distributions. The picture that emerges is that the inefficient energy transfer from the high-frequency CH stretch to the intermolecular modes can take place only from specific orientations and impact parameters and gives rise to restricted energy flow and state-specific vibrational distributions in the fragments.

Acknowledgment. This work is supported by the National Science Foundation. In our work on weakly bound dimers, we benefited greatly from the pioneering work of Prof. R. E. Miller and his deep insights. We would like to thank Colin Western for his generous help in using the PGOPHER program and analyzing the ammonia REMPI results.

References and Notes

(1) Pauling, L. *The Nature of the Chemical Bond and the Structure of Molecules and Crystals: An Introduction to Modern Structural Chemistry*; Cornell University: New York, 1939.

(2) (a) Grabowski, S. J. *Annu. Rep. Prog. Chem., Sect. C*. 2006, 131−165 and references therein. (b) Scheiner, S. *Hydrogen Bonding: A Theoretical Perspective*; Oxford University: New York, 1997.

(3) Miller, R. E. *Science* **1988**, *240*, 447.

(4) Miller, R. E. In *Advances in Laser Science, III*; Tam, A. C., Gole, J. L., Stwalley, W. C., Eds.; Optical Science and Engineering Series 9; Lerner, R. G., Ed.; American Institute of Physics Conference Proceedings: New York, 1988, p 365.

(5) Bohac, E. J.; Miller, R. E. *Phys. Rev. Lett.* **1993**, *71*, 54.

(6) Miller, R. E. In *Chemical Reactions in Clusters*; Bernstein, E. R., Ed.; Oxford University Press: New York, 1996, p 40.

(7) Oudejans, L.; Miller, R. E. *Annu. Rev. Phys. Chem.* **2001**, *52*, 607.

(8) Oudejans, L.; Moore, D. T.; Miller, R. E. *J. Chem. Phys.* **1999**, *110*, 209.

(9) Oudejans, L.; Miller, R. *J. Phys. Chem. A* **1999**, *103*, 4791.

(10) Davey, J. B.; Greenslade, M. E.; Marshall, M. D.; Lester, M. I.; Wheeler, M. D. *J. Chem. Phys.* **2004**, *121*, 3009.

(11) Li, G.; Parr, J.; Fedorov, I.; Reisler, H. *Phys. Chem. Chem. Phys.* **2006**, *8*, 2915.

(12) Fraser, G. T.; Leopold, K. R.; Klemperer, W. *J. Chem. Phys.* **1984**, *80*, 1423.

(13) Hilpert, G.; Fraser, G. T.; Pine, A. S. *J. Chem. Phys.* **1996**, *105*, 6183.

(14) Lin, Y.; Suhm, M. A.; Botschwina, P. *Phys. Chem. Chem. Phys.* **2004**, *6*, 4642.

(15) Spoliti, M.; Bencivenni, L.; Ramondo, F. *J. Mol. Struct. (THEOCHEM)* **1994**, *303*, 185.

(16) Hartmann, M.; Radom, L. *J. Phys. Chem. A* **2000**, *104*, 968.

(17) Ewing, G. E. *J. Chem. Phys.* **1980**, *72*, 2096.

(18) Ewing, G. E. *J. Phys. Chem.* **1987**, *91*, 4662.

(19) McCaffery, A. J. *Phys. Chem. Chem. Phys.* **2004**, *6*, 1637.

(20) McCaffery, A. J.; Marsh, R. J. *J. Chem. Phys.* **2002**, *117*, 9275.

(21) Osborne, M. A.; McCaffery, A. J. *J. Chem. Phys.* **1994**, *101*, 5604.

(22) Kreutz, T. G.; Flynn, G. W. *J. Chem. Phys.* **1990**, *93*, 452.

(23) Dobber, M. R.; Buma, W. J.; deLange, C. A. *J. Phys Chem.* **1995**, *99*, 1671.

(24) Western, C. M. *PGOPHER, A Program for Simulating Rotational Structure*; University of Bristol: Bristol, U.K. http://pgopher.chm.bris.ac.uk.

(25) Eppink, A.; Parker, D. H. *Rev. Sci. Instum.* **1997**, *68*, 3477.

(26) Dribinski, V.; Potter, A. B.; Fedorov, I.; Reisler, H. *J. Chem. Phys.* **2004**, *121*, 12353.

(27) Dribinski, V.; Ossadtchi, A.; Mandelshtam, V. A.; Reisler, H. *Rev. Sci. Instrum.* **2002**, *73*, 2634.

(28) Hollas, J. M. *High Resolution Spectroscopy*, 2nd ed.; Wiley & Sons: Chichester, U.K., 1998.

(29) Slipchenko, M. N.; Vilesov, A. F. *Chem. Phys. Lett.* **2005**, *412*, 176.

(30) Pliva, J. *J. Mol. Spectrosc.* **1972**, *44*, 165.

(31) Sampson, R. K.; Bellm, S. M.; McCaffery, A. J.; Lawrance, W. D. *J. Chem. Phys.* **2005**, *122*, 074311.

(32) McCaffery, J. A.; Osborne, M. A.; Marsh, R. J.; Lawrance, W. D.; Waclawik, E. R. *J. Chem. Phys.* **2004**, *121*, 169.

(33) Parr, J.; Eggert, M.; Fedorov, I.; Reisler, H.; McCaffery, A. J. 2007, submitted for publication.

(34) Palmer, K. F.; Mickelson, M. E.; Rao, K. N. *J. Mol. Spectrosc.* **1972**, *44*, 131.